Molecular Catalysis 443 (2017) 131–138

Contents lists available at ScienceDirect

Molecular Catalysis

journal homepage: www.elsevier.com/locate/mcat

MCAT

Research Paper

Surface oxygen vacancies dominated CeO_2 as efficient catalyst for imine synthesis: Influences of different cerium precursors

Jingjin Zhang[a], Jingxia Yang[a,b,*], Jinjie Wang[a], Huihui Ding[a], Qianlong Liu[a], Ulrich Schubert[b], Yichuan Rui[a], Jingli Xu[a]

[a] College of Chemistry and Chemical Engineering, Shanghai University of Engineering Science, LongTeng Road 333, 201620 Shanghai, PR China
[b] Institute of Materials Chemistry, Vienna University of Technology, Getreidemarkt 9, 1060 Wien, Austria

ARTICLE INFO

Article history:
Received 19 June 2017
Received in revised form 7 September 2017
Accepted 27 September 2017

Keywords:
Ceria catalyst
Precursor influences
Ethylene glycol
Imine synthesis
Surface oxygen vacancy

ABSTRACT

CeO_2 as catalysts for imine synthesis was synthesized from three different inorganic precursors ($Ce(OH)_4$, $Ce(COOCH_3)_3{\cdot}5H_2O$ and $Ce(NO_3)_3{\cdot}6H_2O$) in ethylene glycol (EG) as solvothermal solvent. The influences of some parameters were investigated, such as the surfactant polyvinylpyrrolidone (PVP), H_2O as co-solvent, and CH_3COOH or NaOH as mineralizer (exclusive for $Ce(NO_3)_3$ as the precursor). The different precursors influenced the coordination of EG with cerium, crystalline, surface structure and also the catalytic ability for imine synthesis. The highest imine conversion rate was obtained when CeO_2 was synthesized from $Ce(NO_3)_3$ + PVP + CH_3COOH +EG. The mechanism was investigated by carefully checking the structures of the synthesized CeO_2, such as XRD, morphology, surface area, XPS and so on, and figured out that the high catalytic activity of the best CeO_2 sample was much more related with the high proportion of surface oxygen vacancies than the surface area and the Ce^{3+} ratio.

1. Introduction

CeO_2 is a well-known catalytic material due to its high oxygen storage and release capacity related to the Ce^{3+}-Ce^{4+} redox cycle·CeO_2 based materials have been widely used as CO oxidation catalyst (e.g [1,2]), NO_x reduction catalyst ([3–5]), photocatalyst ([6,7]) and also very recently as catalyst for imine synthesis ([8–11]). Two properties are very important for CeO_2 as a catalyst: (a) a high Ce^{3+} proportion, and (b) a high surface area, providing more reaction sites. Thus, much effort has been spent on these two aspects, and varying the ceria precursor is one possibility ([2,12]). Qi et al. proved that the use of $Ce(NO_3)_3$ or $(NH_4)_2Ce(NO_3)_6$ as precursor can influence the content of Ce^{3+} in the synthesized CeO_2 and the catalytic ability for CO oxidation [13], and $Ce(NO_3)_3$ yielded CeO_2 with a higher Ce^{3+} proportion. We previously used cerium *tert*-butoxide ($Ce(O^tBu)_4$) as precursor and synthesized CeO_2 with very high surface area (up to 277 m^2/g) [14]. and with graphene-like residues [15].

During previous syntheses, solvothermal processing proved to be a convenient and efficient way to get CeO_2 with high surface area. Ethylene glycol (EG) has been used as solvent on many occasions (e.g [16–18]) because of its high boiling point. Previous reports also indicated that $Ce(OH)_4$ can form $Ce(EG)_2$ under certain condition [19,20], and cerium glycolate was already used as precursor to synthesize CeO_2 [21–23]. Recently, EG was used as chelating agent for $Ce(NO_3)_3$ and influenced the synthesized CeO_2-(ZrO_2)-Al_2O_3 composite materials [17]. It was hardly investigated how different cerium salts influence the properties of CeO_2 prepared under solvothermal condition in EG, and how the structural changes would influence the catalytic activity in imine synthesis (firstly reported in 2015 by M. Tamura et al. [8]). Imine is an important intermediate in the synthesis of various biological, agricultural, and pharmaceutical compounds. The use of CeO_2 as catalyst is more easily to separate than the conventional catalyst such as KOH, NaOH, and DABCO [8], and it can be used at low temperature. There are also some literatures using oxides (eg. MnOx) based catalysts [24–27]. for imine synthesis, which were also easy to separate. But they functioned mostly at above 100 °C, and at low temperature the conversion of imine was very low [8].

This research focuses on the preparation and characterization of CeO_2 from different cerium precursors in EG system, and the imine synthesis was used to check the catalytic ability of the synthesized CeO_2. Three different inorganic cerium compounds ($Ce(OH)_4$, $Ce(COOCH_3)_3{\cdot}5H_2O$ and $Ce(NO_3)_3{\cdot}6H_2O$) were used as starting materials in solvothermal syntheses with EG as solvent and

* Corresponding author at: College of Chemistry and Chemical Engineering, Shanghai University of Engineering Science, LongTeng Road 333, 201620 Shanghai, PR China.
E-mail addresses: yjx09tj@foxmail.com, jxyang@sues.edu.cn (J. Yang).

http://dx.doi.org/10.1016/j.mcat.2017.09.030
2468-8231/

Table 1
Solution composition and particle size of different samples.

No.	Ceria precursor (amount)	Surfactant (amount)	H_2O	Mineralizer	Particle size (By DLS)
1	$Ce(OH)_4$ (5 mmol)	/	/	/	228 ± 15
2.	$Ce(OH)_4$ (5 mmol)	PVP (1.5 g)	/	/	271 ± 29
3	$Ce(COOCH_3)_3{\cdot}5H_2O$ (5 mmol)	PVP (1.5 g)	/	/	1674 ± 306
4	$Ce(NO_3)_3{\cdot}6H_2O$ (5 mmol)	PVP (1.5 g)	/	CH_3COOH (2 mL)	294 ± 10
5	$Ce(NO_3)_3{\cdot}6H_2O$ (5 mmol)	PVP (1.5 g)	Yes (10 mL)	CH_3COOH (2 mL)	392 ± 22
6	$Ce(NO_3)_3{\cdot}6H_2O$ (5 mmol)	PVP (1.5 g)	Yes (10 mL)	NaOH (4.8 g)	249 ± 19

polyvinylpyrrolidone (PVP) as surfactant to stabilize small CeO_2 particles and thus provide high surface areas. For $Ce(NO_3)_3{\cdot}6H_2O$, the effects of H_2O and different mineralizer were also investigated. The properties of the synthesized CeO_2 were checked by IR, TGA, XRD, XPS and BET. The materials were used as catalyst for imine synthesis at low temperatures (room temperature, 25 °C), and the imine formation rate was used to characterize the catalytic ability of CeO_2. Finally, the parameters influencing the CeO_2 catalytic activity were analyzed and the mechanism of CeO_2 during imine formation was proposed.

2. Experimental section

2.1. CeO_2 synthesis

All chemicals were AR grade from adamas reagent Co., and used as received. $Ce(OH)_4$, $Ce(COOCH_3)_3{\cdot}5H_2O$ and $Ce(NO_3)_3{\cdot}6H_2O$ were used as precursors. Ethylene glycol was used as solvent, while PVP (k 10–15) was used as surfactant.

In a typical synthesis, the ceria precursor (5 mmol) was dissolved in 50 mL of ethylene glycol (EG). Then 1.5 g of PVP was added and the mixture stirred for 30 min. To the samples prepared from $Ce(NO_3)_3{\cdot}6H_2O$ as the precursor, a mineralizer was added. The solution was then transferred into an autoclave with Teflon inline (100 mL). The autoclave was sealed and kept at 190 °C for 6 h. After cooling to room temperature naturally, the suspension was centrifuged at 9500 rpm and the solid residue washed three times with ethanol. The obtained powders were dried in vacuum at 60 °C for at least 12 h. Part of the samples were calcined at 500 °C for 1 h (heating rate: 2 °C/min). The starting mixtures of the different samples are listed in Table 1.

2.2. CeO_2 characterization

The surface groups of CeO_2 were characterized by Fourier transform infrared spectra (FT-IR) using a Perkin-Elmer Spectrum one spectrometer. The XRD patterns were recorded with a Shimadzu (Japan) D/Max-2500 diffractometer using monochromatized, nickel-filtered $Cu_{K\alpha}$ radiation. The morphology of the CeO_2 samples was observed using a scanning electron microscope (SEM, Hitachi S-8000, Japan) in a secondary electron scattering mode at 5 kV. Thermogravimetric/differential thermal analysis (TG-DTA) was performed on a NETZSCH STA2500 from room temperature to 800 °C in air with 10 °C/min ramping rate. Dynamic light scattering (DLS) were used to determine the particle size, by using PSS Nicomp 380 at 25C with the measurement angle of 173 (back scatter). Samples were ultrasonically dispersed in ethanol for 15 min and then left standing 2 min for balancing. Mean diameters were obtained from three measurements. N_2 adsorption/desorption was measured at 77 K by using a Micromeritics ASAP 2020 instrument. All samples were degassed at 120 °C for at least 5 h before testing. The specific surface area was obtained by the BET method, and the pore size distribution was calculated from the desorption branch of the isotherm. X-ray photoelectron spectra (XPS) were recorded with a Thermo Fisher ESCALAB 250 xi (England) using $Al_{K\alpha}$ radiation (1486.6 eV). Binding energies were calculated with respect to C(1s) at 284.8 eV. Binding energies were measured with a precision of ±0.05 eV. Before XPS test, all samples were calcined at 500 °C for 1 h in the air to clean the surface. Then the samples were kept in glove box (H_2O < 1 ppm) until XPS test. The Ce:O ratio was calibrated by using a standard CeO_2 from Sigma-Aldrich. XPS data were analyzed using XPSPEAK 4.1 software, and all the fitted peaks were of a Gaussian-Lorentzian shape. The relative standard deviation $\Sigma\chi^2$ were below 10.

2.3. Catalytic experiments

The catalytic test was modified based on the design of Tamura [8]. Benzyl alcohol (10 mmol) and aniline (20 mmol) were put in a reaction tube under air without solvent. Then 50 mg CeO_2 was added and stirred vigorously at 500 rpm at room temperature (ca. 25 °C). For conversion detection, the reaction mixture was centrifuged, and the liquids were transferred to new vials. The products were diluted in ethanol and analyzed by using a Shimadzu GC2014 plus equipped with an Rxi-5 ms capillary column and a flame ionization detector. In order to compare with the other researches, the reaction rates were used to characterize the catalytic ability, by calculating the imine formation amount per hour per catalyst amount (mmol h^{-1} g^{-1}).

3. Results and discussion

3.1. Structure characterization of CeO_2 catalysts

The influence of different precursors can be seen firstly from the color of the solvothermally treated solution (Fig. 1 right). Samples 1 and 2 with light brown color were prepared from $Ce(OH)_4$, without and with PVP, respectively. Yellowish-white sample 3 was synthesized from $Ce(COOCH_3)_3$. $Ce(NO_3)_3$ was used as precursor for samples 4–6, but with different solvent and mineralizer, exhibiting very different colors: black (CH_3COOH), brown ($H_2O + CH_3COOH$) and white (H_2O + NaOH).

After the samples had been centrifuged and dried overnight, IR spectra were taken to characterize their surface (Fig. 1 left). All samples had bands at 2849 and 2925 cm^{-1}, corresponding to CH_2 and CH_3 vibrations, caused by residual PVP and EG. Sample 6 showed the weakest signals at these two positions. Furthermore, the samples prepared without external H_2O (samples 1–4) exhibited a sharp peak at 1085 cm^{-1}, which corresponds to C—O vibrations. This information proved that EG is coordinated to Ce through Ce—O—C bonds. H_2O accelerates the breaking of these bonds through hydrolysis reactions. Carbon-containing groups on

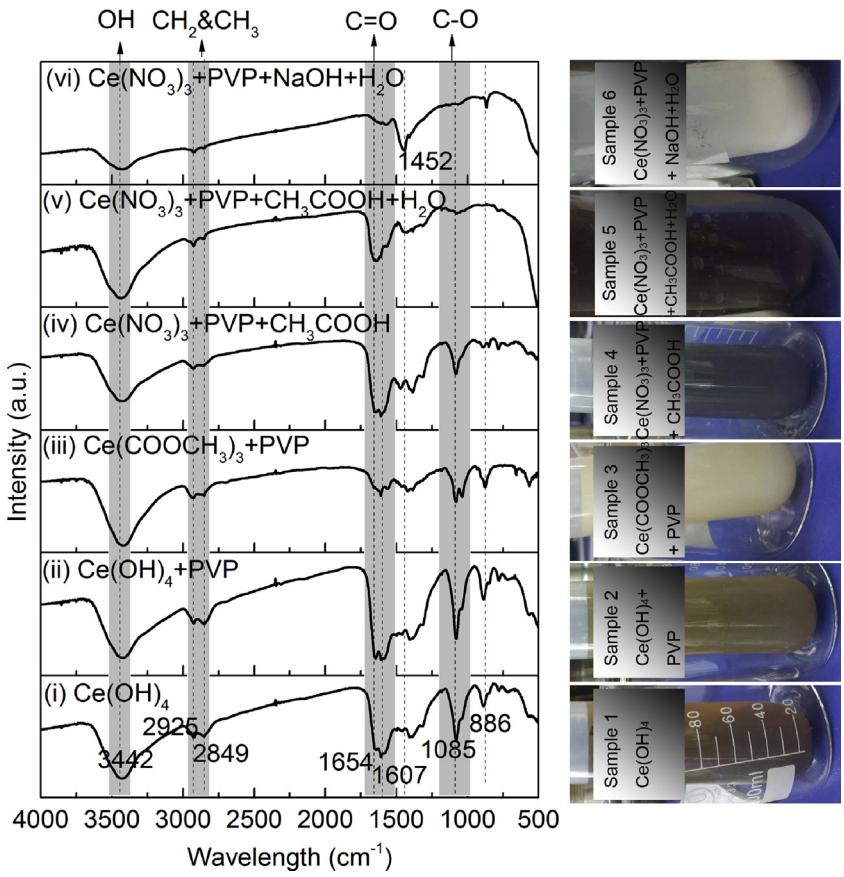

Fig. 1. FT-IR spectra (left) and solution color (right) of different as-prepared CeO_2 samples:(i) $Ce(OH)_4$, (ii)$Ce(OH)_4$ + PVP, (iii)$Ce(COOCH_3)_3$ + PVP, (iv)$Ce(NO_3)_3$ + CH_3CHOOH + PVP, (v)$Ce(NO_3)_3$ + CH_3CHOOH + PVP + H_2O, (vi)$Ce(NO_3)_3$ + NaOH + PVP + H_2O.

the surface of CeO_2 result in vibrations at 1607 and 1654 cm^{-1}. This is similar as in a previous study using ethanol as solvent [14].

Coordination of EG can be further proven by TG-DTA analysis (Fig. 2). Except sample 6, all samples gave large weight loss and heat release at ca. 250 °C. The weight loss was almost the same when external H_2O was not involved during the synthesis and was in the range of 30–40% for samples 1–4. When external H_2O was added to the solvothermal solvent, the intensity of heat release peak decreased dramatically, from ca. 30 W/g to only 2–4 W/g, and the weight loss of sample 5 and 6 was also reduced to only 11% and 9%, respectively. These results prove the coordination of EG to Ce, and that H_2O can break the bonds between Ce and EG, resulting in less carbon-containing residues.

The as-prepared and calcined samples were also characterized by XRD (Fig. 3). The diffraction peak intensities were different for as-prepared samples from different precursors (Fig. 3 left). Furthermore, samples from $Ce(OH)_4$ consisted only of CeO_2 as the crystalline phase (PDF No: 34-0394), while the use of $Ce(COOCH_3)_3{\cdot}5H_2O$ and $Ce(NO_3)_3{\cdot}6H_2O$ yielded additionally Ce_2O_3 as crystalline phase. For $Ce(NO_3)_3{\cdot}6H_2O$ as the precursor, the intensity of the diffraction peaks increased slightly by the addition of H_2O, and enhanced greatly when NaOH was used as mineralizer instead of CH_3COOH. After calcination at 500 °C for 1 h (Fig. 3 right), all samples were pure CeO_2, only the crystalline particle sizes varied in the range of 7.2–9.7 nm.

The images of the synthesized CeO_2 samples are shown in Fig. 4. When there was no external H_2O in the solvothermal solvent, only sample 3 with $Ce(COOCH_3)_3$ as the precursor resulted in large particles, which were about 150–300 nm in diameter. Samples 1&2 had small particles of 10–20 nm in diameter, and 30–40 nm for sample 4. These sizes are larger than the crystalline particle sizes in Fig. 3, but much smaller than the DLS particle size in Table 1. This suggested that the particles in SEM images are agglomerations of small crystalline particle (7.2–9.7 nm) and can further aggregate in ethanol. The agglomeration of particles may reduce the surface area and the total surface oxygen vacancies. When H_2O was added to the $Ce(NO_3)_3$ system using PVP as surfactant (sample 5) large particles of 400 nm in diameter were obtained, in agreement with the DLS measurements. The formation of large spheres was because of PVP surfactant, reaching a critical micelle concentration when both H_2O and CH_3COOH existed. Taking the crystalline particle sizes in Fig. 3 into account, the material must also be agglomerated. Use of NaOH as mineralizer, and PVP as surfactant (sample 6) resulted in small particles of 10–20 nm in diameter.

All samples calcined at 500 °C for 1 h were characterized by XP spectra (Fig. 5) and N_2 sorption, the results were summarized in Table 2. For XPS test, all the samples were pre-treated in the air at 500 °C for 1 h to clean the surface including H_2O. Then they were kept in glove boxes before XPS test. The H_2O of the glove box is <1 ppm. As the catalytic ability of CeO_2 is closely related to the Ce^{3+} proportion, the Ce 3d region of XP spectra is shown in Fig. 5 left. The Ce 3d region contains five doublets (v denotes Ce 3d5/2, u denotes Ce 3d3/2). v^0, v′, u^0, u′ belong to Ce^{3+} species, whereas v, v″, v‴, u, u‴ and u‴ belong to Ce^{4+} species [28]. To calculate the $Ce^{3+}/(Ce^{3+}+Ce^{4+})$ ratio (abbreviated "Ce^{3+} ratio"), the peak area of the u^0 (v^0) and u′ (v′) relative to the area of the entire Ce 3d region was determined [13]. All the synthesized CeO_2 samples possessed much higher Ce^{3+} ratios than commercial CeO_2 (5%). Except sample 1 with a relatively low Ce^{3+} ratio (ca. 11.5%), all the other samples had a Ce^{3+} ratio of about 20%, suggesting that the use of EG and PVP was beneficial for increasing the Ce^{3+} ratio. The ceria precursor had almost no influence on the Ce^{3+} ratio.

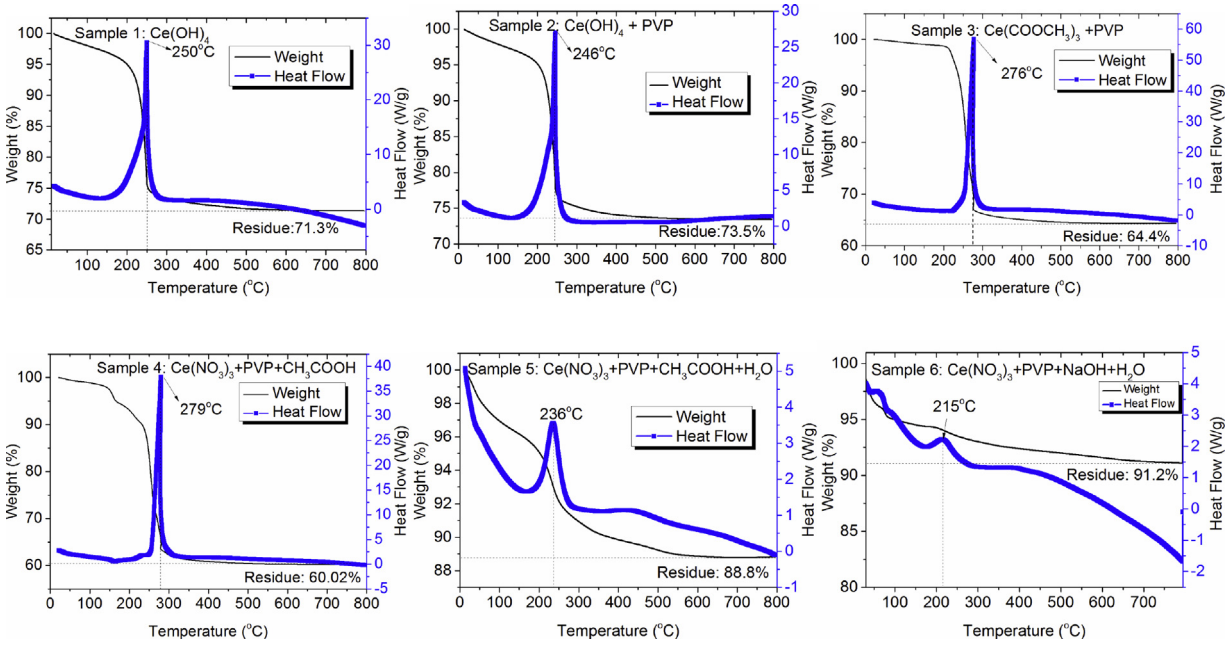

Fig. 2. TG-DTA curves of different as-prepared samples.

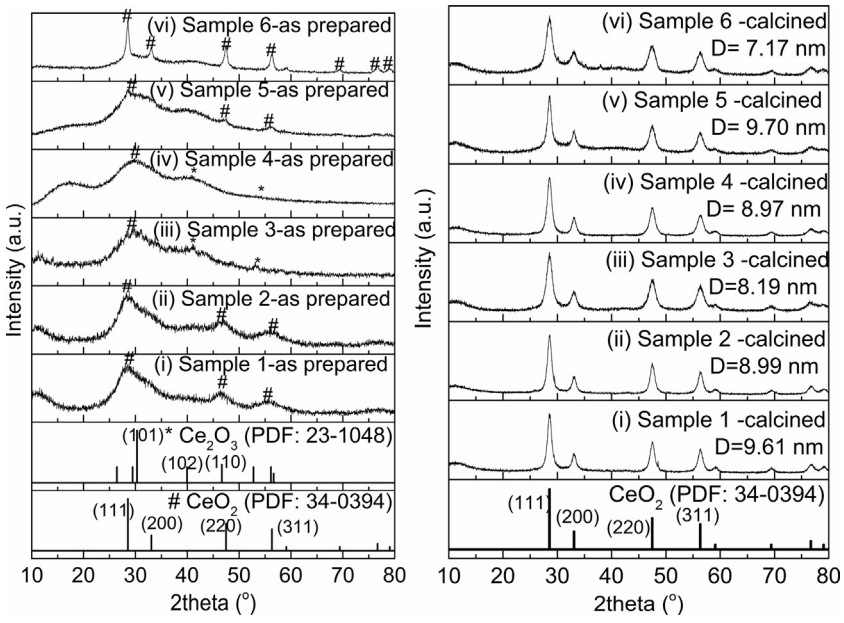

Fig. 3. XRD pattern of different as-prepared(left) and calcined (right) CeO_2 samples:(i) $Ce(OH)_4$, (ii) $Ce(OH)_4$ + PVP, (iii) $Ce(COOCH_3)_3$ + PVP, (iv) $Ce(NO_3)_3$ + CH_3CHOOH + PVP, (v) $Ce(NO_3)_3$ + CH_3CHOOH + PVP + H_2O, (vi) $Ce(NO_3)_3$ + NaOH + PVP + H_2O. The crystalline particle sizes were evaluated by the Scherrer formula based on the strongest peak (111) of CeO_2 at ca. 2theta = 28.5°.

Table 2
Summary of XPS and N_2 sorption results for CeO_2 samples calcined at 500 °C for 1 h.

Sample No.	XPS test						N_2 sorption	
	Ce3d (Atomic%)	O1s (Atomic%)	Ce^{3+} ratio(%)	O% of H_2O(%)	O/Ce	terminal O/Ce *	S_{BET}(m^2/g)	D_{BJH}(nm)
1	25.27	74.73	11.5	10.8	2.96	2.79	127.8	6.9
2	33.58	66.42	20.2	1.0	1.98	1.68	129.0	4.9
3	33.26	66.74	21.5	1.2	2.01	1.69	132.9	5.8
4	**34.14**	**65.86**	**20.1**	**0.3**	**1.93**	**1.63**	**175.8**	**4.7**
5	33.74	66.26	19.7	0.7	1.96	1.66	87.2	9.4
6	32.64	67.36	20.6	4.2	2.06	1.75	136.2	4.9

* Terminal O/Ce = O/Ce-1.5Ce^{3+}%.

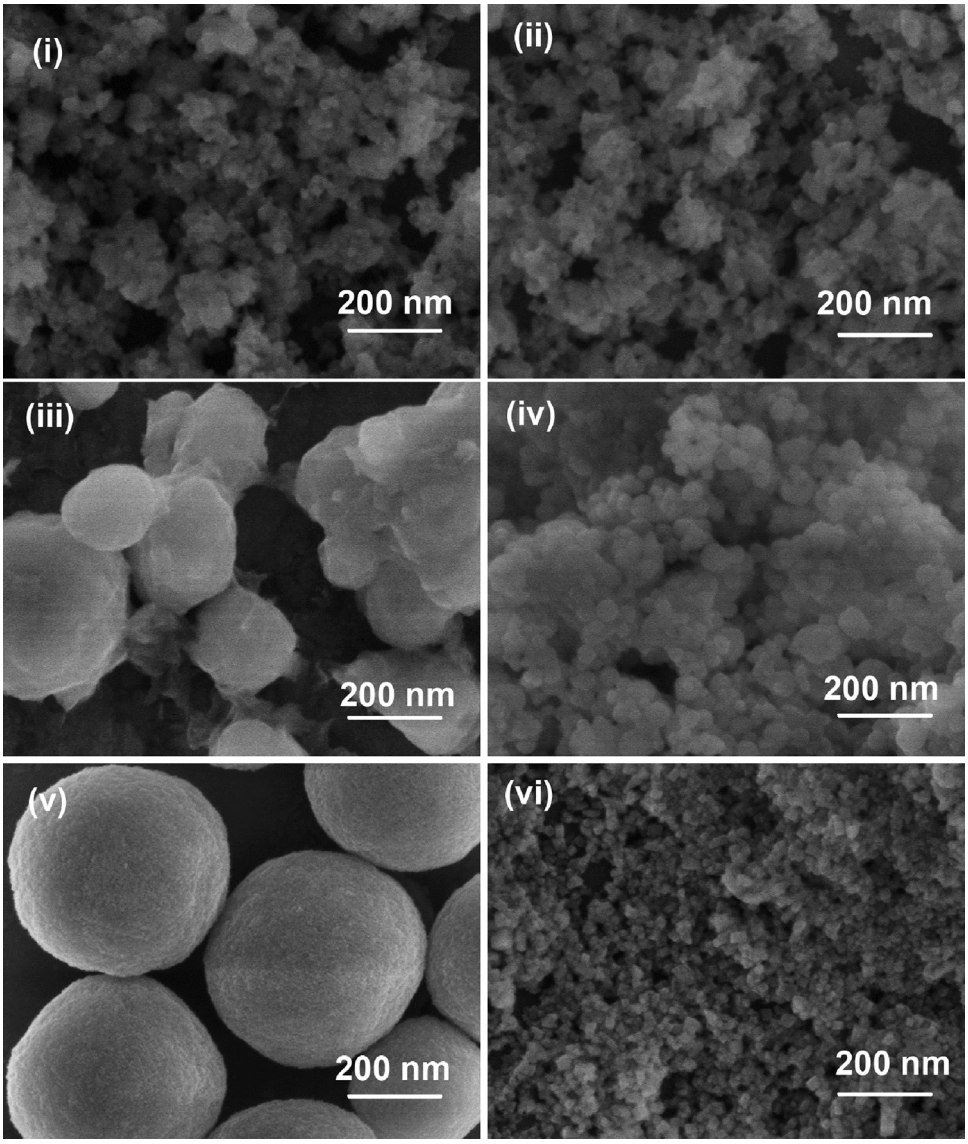

Fig. 4. SEM images of different as-prepared samples (i) $Ce(OH)_4$, (ii) $Ce(OH)_4$ + PVP, (iii) $Ce(COOCH_3)_3$ + PVP, (iv) $Ce(NO_3)_3$ + CH_3CHOOH + PVP, (v) $Ce(NO_3)_3$ + CH_3CHOOH + PVP + H_2O, (vi) $Ce(NO_3)_3$ + NaOH + PVP + H_2O.

The amount of oxygen vacancies on CeO_2 surface can be deducted by the O1 s results. It has been reported that H_2O prefers to stay on the lattice oxygen on the surface, and the surface oxygen vacancies on CeO_2 (111) surface suppressed the formation and adsorption of H_2O by surface hydroxyl as proposed both experimentally and theoretically [29–34]. As all the samples in this experiment were calcined in the air at 500 °C for 1 h and kept in glove boxes before XPS test. The detected H_2O signal was from the transformation of surface hydroxyl or chemisorbed H_2O. Thus the amount of H_2O on the surface can be used to express the number of surface oxygen vacancies. The less H_2O exists, the higher amount is the surface oxygen vacancy. When focusing on the O 1 s XP spectra (Fig. 5 right), the region can be fitted to three peaks: (1) 533.1 eV, corresponding to H_2O physically/chemically adsorbed on the CeO_2 surface; (2) 531.4 eV, assigned to OH* chemically absorbed on the CeO_2 surface; (3) 529.3 eV, belonging to CeO_2. By calculating the area of each peak, the O% of H_2O for the synthesized samples are: sample 1 (10.8%) > sample 6 (4.2%) > sample 3 (1.2%) > sample 2 (1.0%) > sample 5 (0.7%) > sample 4 (0.3%), indicating that sample 4 had the most oxygen vacancies on the surface.

The surface oxygen vacancies can also be proven by the O/Ce ratio (Table 2). Basically, the higher the Ce^{3+} ratio is, the lower is the O/Ce ratio. In Table 2 the reverse trends is found. For example, when sample 4 is compared with sample 3, the Ce^{3+} ratio of sample 4 is 20.1%, lower than 21.5% of sample 3. In principle, the O/Ce ratio of sample 4 should be somewhat higher than that of sample 3. But the detected O/Ce ratio was 1.93 for sample 4 and 2.01 for sample 3. This is probably due to the penetration depth (about 10 nm) of XPS, which is a surface analysis method. Considering that the crystallite sizes of all samples were in the range of 7.2–9.7 nm (Fig. 3), the detection can penetrate one whole crystalline particle and reach the surface of another crystalline particle. Thus the kind of surface atom can theoretically influence the O/Ce ratio, and it can be used as a reference to evaluate the relative amount of surface oxygen vacancies. By subtracting the influence of Ce^{3+} on the O/Ce ratio (O/Ce-1.5Ce^{3+}%, named as terminal O/Ce), the lower terminal O/Ce ratio indicates less oxygen as surface-terminating atom. The sequence of terminal O/Ce ratio is sample 1 (2.79) > sample 6 (1.75) > sample 3 (1.69) > sample 2 (1.68) > sample 5 (1.66) > sample 4 (1.63), in the same sequence of O% (H_2O) in Fig. 5 right. This proved that sample 4 had the lowest O proportion as terminal atoms and

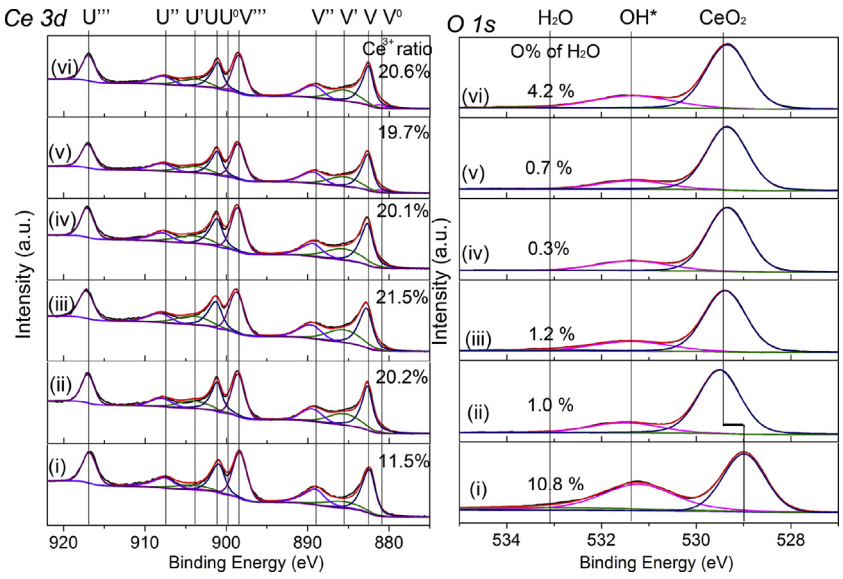

Fig. 5. XP spectra of the Ce 3d region(left) and O 1 s region (right) for CeO_2 samples calcined at 500 °C for 1 h. (i) $Ce(OH)_4$, (ii) $Ce(OH)_4$ + PVP, (iii) $Ce(COOCH_3)_3$ + PVP, (iv) $Ce(NO_3)_3$ + CH_3CHOOH + PVP, (v) $Ce(NO_3)_3$ + CH_3CHOOH + PVP + H_2O, (vi) $Ce(NO_3)_3$ + NaOH + PVP + H_2O.

most oxygen vacancies on the surface. When $Ce(NO_3)_3$ was used as precursor, adding of H_2O or NaOH as mineralizer increased the proportion of terminal O atoms, suggesting that the amount of surface oxygen vacancies decreased. The Na content was also checked by XPS, and there was almost no Na residue. The reason for the very high O/Ce ratio of sample 1 is not clear; perhaps the absence of PVP had some influence.

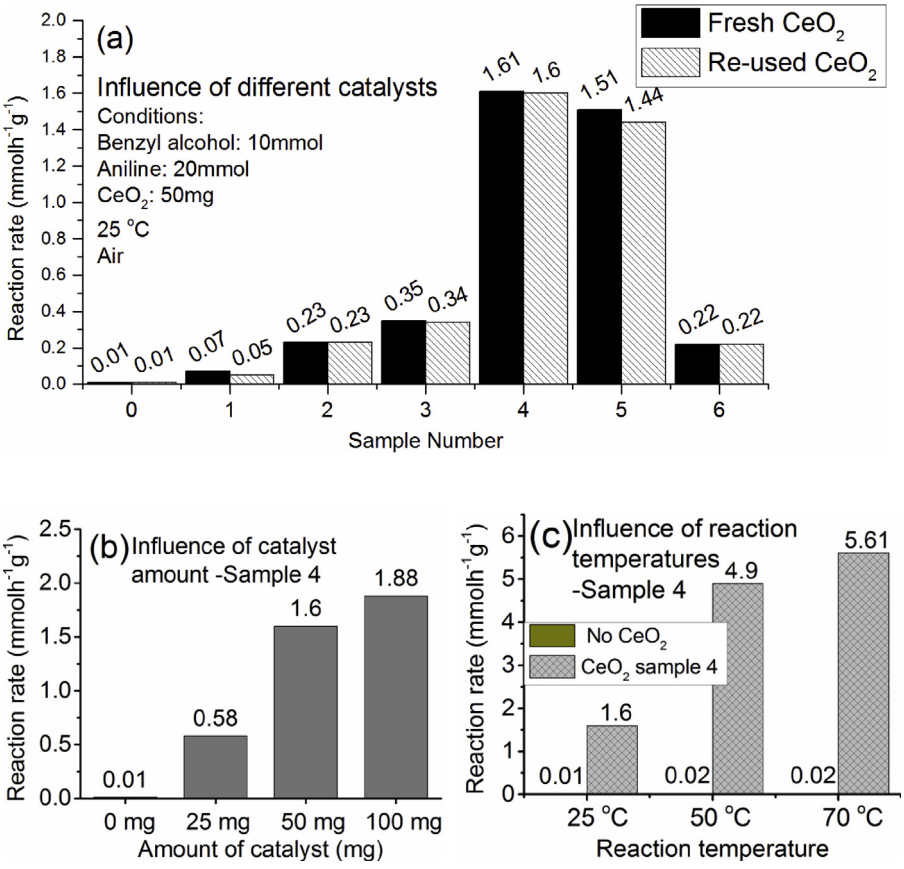

Fig. 6. Reaction rates of different samples, indicating the imine formation rate per catalyst amount per hour; all the values were calculated with conversion below 20%.
(a) Influences of different CeO_2 samples, (0)Without catalyst, (1) $Ce(OH)_4$, (2) $Ce(OH)_4$ + PVP, (3) $Ce(COOCH_3)_3$ + PVP, (4) $Ce(NO_3)_3$ + CH_3CHOOH + PVP, (5) $Ce(NO_3)_3$ + CH_3CHOOH + PVP + H_2O, (6) $Ce(NO_3)_3$ + NaOH + PVP + H_2O.
(b) Influences of catalyst loading, by using sample 4 as an example.
(c) Influences of reaction temperature, by using sample 4 as an example.

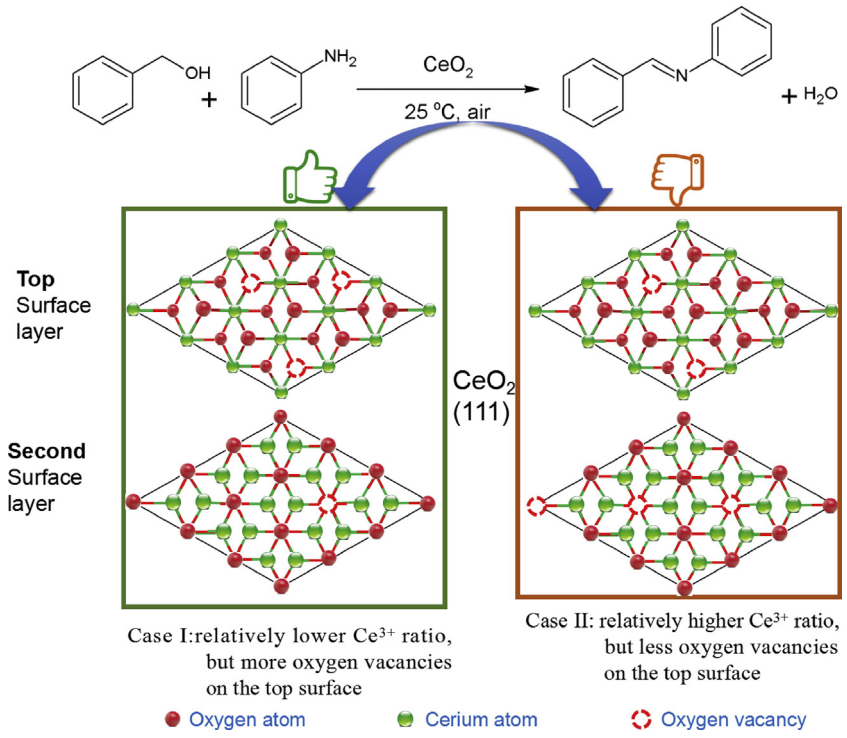

Fig. 7. Proposed mechanism of efficient CeO_2 catalyst for imine synthesis.

All N_2 adsorption – desorption isotherms (Fig. S1) belong to IUPAC type IV classification [35], indicating that the synthesized CeO_2 samples were mesoporous. In the absence of H_2O, the highest surface area of 175.8 m^2/g belonged to CeO_2 from $Ce(NO_3)_3$, and the lowest of 128 m^2/g to that from $Ce(OH)_4$. The use of PVP did not increase the surface area for $Ce(OH)_4$ as precursor, but can increase the Ce^{3+} ratio. The N_2 adsorption – desorption results indicated that the ceria precursor can influence the surface area. For $Ce(NO_3)_3$, addition of H_2O decreased the surface area (from 175.8 m^2/g to 87.2 m^2/g) of CeO_2, which may not only be related to the hydrolysis of Ce—O—C bonds (as indicated in TGA results), but also influenced by the change of CeO_2 morphology (with H_2O, the sample consisted of large spheres of 400 nm in diameter, rather than 30–40 nm small particles in the pure EG system). The change of mineralizer can also influence the surface area, but has almost no influence on the Ce^{3+} ratio.

3.2. Catalytic test of CeO_2

All samples were used as catalysts for imine synthesis, as summarized in Fig. 6. An amount of 10 mmol of benzyl alcohol and 20 mmol of aniline were put in a test tube, using 50 mg CeO_2 as the catalyst (Fig. 6(a)). The experiments were carried out at room temperature (ca. 25 °C) in natural light for at least 3 h. The reaction rate is used to express the catalytic ability of CeO_2, by calculating the imine formation per catalyst amount per hour using the conversion below 20%. The reaction rate sequence was sample 4 (1.61 mmol h^{-1} g^{-1}) > sample 5 (1.51 mmol h^{-1} g^{-1}) > sample 3 (0.35 mmol h^{-1} g^{-1}) > sample 2 (0.23 mmol h^{-1} g^{-1}) > sample 6 (0.22 mmol h^{-1} g^{-1}) > sample 1 (0.05 mmol h^{-1} g^{-1}). The highest reaction rate 1.61 mmol h^{-1} g^{-1} belongs to sample 4, much higher than the reported 0.46 mmol h^{-1} g^{-1} [8]. The used CeO_2 were collected and heated at 500 °C for 1 h, and re-used for imine synthesis again. The reaction rates were almost the same as those of fresh CeO_2.

The adsorption influence of catalyst was also studied by using the best sample 4 (Fig. 6(b)). When the catalyst amount changed from 25 mg to 50 mg and to 100 mg, the reaction rate increased from 0.58 mmol h^{-1} g^{-1} to 1.6 mmol h^{-1} g^{-1} and then to 1.88 mmol h^{-1} g^{-1}. This may be because the prepared CeO_2 was of mesoporous structure, and can adsorb the reactant or intermediate, blocking the active sites of CeO_2 catalyst. The desorbing of adsorbate probably needed a while to reach a balance. Thus more CeO_2 loading can provide more active sites and the adsoring-desorbing can reach a faster balance.

The influences of temperature were also studied by using the best sample (No. 4). Three different temperatures (25 °C, 50 °C, and 70 °C) were used and calculated the reaction rates (Fig. 6(c)). When the temperature rise from 25 °C to 50 °C, the reaction rate increased from 1.6 mmol h^{-1} g^{-1}–4.9 mmol h^{-1} g^{-1}, increasing to more than 3 times. Further increase the temperature to 70 °C, the reaction rate only improved slightly to 5.61 mmol h^{-1} g^{-1}.

3.3. Catalytic mechanism of CeO2 as imine catalyst

Compared with the reaction without catalyst (sample 0, 0.01 mmol h^{-1} g^{-1}), the use of CeO_2 prepared from $Ce(NO_3)_3$ can improve the conversion greatly (sample 4, 1.6 mmol h^{-1} g^{-1}). It is clear for sample 4 because of the high surface area and relatively high Ce^{3+} ratio. But for sample 5, the results are difficult to explain just from conventional surface area and Ce^{3+} ratio parameters. It had a lower surface area (87.2 m^2/g) and a smaller Ce^{3+} ratio (19.7%) than those of sample 3 (132.9 m^2/g, 21.5%), but a rather higher reaction rate of 1.51 mmol h^{-1} g^{-1} compared with 0.35 mmol h^{-1} g^{-1} of sample 3. This is perhaps related to the amount of oxygen vacancies on the surface. In Table 2 and Fig. 5, the amount of surface oxygen vacancies was evaluated from the O% of H_2O by XPS fitting and from the terminal O/Ce ratio after removing the influence of the Ce^{3+} stoichiometry. The concentration of surface oxygen vacancies was the almost same sequence (except sample 2 and 3) as the imine

formation rate: sample 4 > sample 5 > sample 2 > sample 3 > sample 6 > sample 1 (the reaction rate of sample 3 was 0.35 mmol h^{-1} g^{-1}, a little bit higher than 0.23 mmol h^{-1} g^{-1} of sample 2, which may be because sample 3 was with a higher surface area.). Thus, the conversion is probably greatly related with the amount of oxygen vacancies on the surface.

It's well known that CeO_2 is very easy to lose O to form oxygen vacancies, and oxygen vacancies of CeO_2 can react with O_2 to form active oxygen atom O*. This may happen similar during imine synthesis. It has been proved that O_2 is necessary during imine synthesis by using CeO_2 as catalyst [8]. The oxygen vacancies of CeO_2 can generate active oxygen atom O* (Eq. (1)), and O* can react with benzyl alcohol to form benzaldehyde and OH* radical (Eq. (2)). The OH* radical will attack aniline to form H_2O and an intermediate (Eq. (3)), which will react fast with benzaldehyde to form imine (Eq. (4)). As the bulk oxygen vacancies are not easily to get access to O_2 and the reactant or intermediate, and at low temperature the migration of bulk oxygen vacancies is not fast, the amount of surface oxygen vacancies is more important. This has also been proved in toluene oxidation by using CeO_2 as catalyst [36]. Thus, the more oxygen vacancies (less O atoms) on the surface are, the higher is the CeO_2 catalytic ability for imine synthesis, as sketched in Fig. 7.

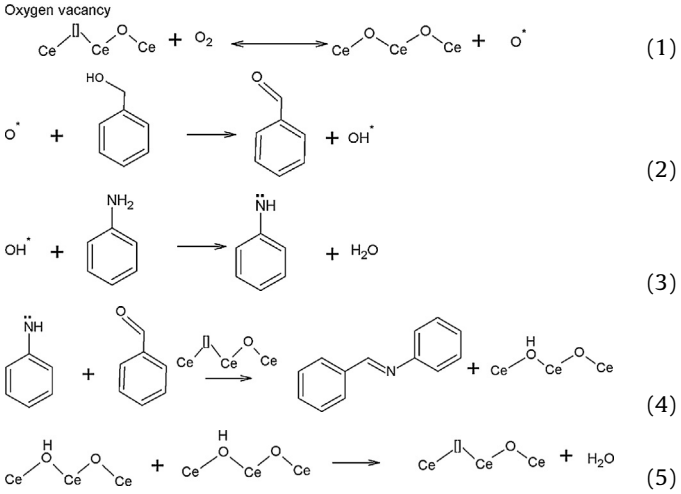

4. Conclusions

CeO_2 was synthesized from three different inorganic precursors ($Ce(OH)_4$, $Ce(COOCH_3)_3{\cdot}5H_2O$ and $Ce(NO_3)_3{\cdot}6H_2O$) and used as catalyst for imine synthesis. The results indicated that $Ce(NO_3)_3$ was the best precursor to obtain the most effective CeO_2 catalyst. The use of pure EG as solvent and CH_3COOH as mineralizer were beneficial to enhance the catalytic ability, comparing with EG + H_2O as solvent and NaOH as mineralizer. The relative amount of surface oxygen vacancies was evaluated from the O% of H_2O in O 1 s peak fitting and the O/Ce ratio subtracting 1.5 Ce^{3+}%. It was found that the sample from $Ce(NO_3)_3$ + EG + PVP + CH_3COOH had relatively more surface oxygen vacancies than the other samples. This is probably the reason of high catalytic ability besides high surface area and high Ce^{3+} ratio.

Acknowledgments

Thanks to Dr. H. Li for the kind assistance of XPS analysis. This research is supported by the program of Shanghai "Young Eastern Scholar"(grant number QD2016037), National Natural Science Foundation of China (grant number 21601121), and the Startup Foundation for Docotors of Shanghai University of Engineering Science (grant number 2016-21).

Appendix A. Supplementary data

Supplementary data associated with this article can be found, in the online version, at http://dx.doi.org/10.1016/j.mcat.2017.09.030.

References

[1] L. Lukashuk, K. Foettinger, E. Kolar, C. Rameshan, D. Teschner, M. Haevecker, A. Knop-Gericke, N. Yigit, H. Li, E. McDermott, M. Stoeger-Pollach, G. Rupprechter, J. Catal. 344 (2016) 1–15.
[2] J. Yang, L. Lukashuk, J. Akbarzadeh, M. Stoeger-Pollach, H. Peterlik, K. Foettinger, G. Rupprechter, U. Schubert, Chem. Eur. J. 21 (2015) 885–892.
[3] P.A. Kumar, Y.E. Jeong, H.P. Ha, Catal. Today 293 (2017) 61–72.
[4] Y.E. Jeong, P.A. Kumar, H.P. Ha, K.-y. Lee, Catal. Lett. 147 (2017) 428–441.
[5] J. Xu, G. Lu, Y. Guo, Y. Guo, X.-Q. Gong, Appl. Catal. A 535 (2017) 1–8.
[6] S. Kumar, A.K. Ojha, RSC Adv. 6 (2016) 8651–8660.
[7] S. Phanichphant, A. Nakaruk, D. Channei, Appl. Surf. Sci. 387 (2016) 214–220.
[8] M. Tamura, K. Tomishige, Angew. Chem. 54 (2015) 864–867.
[9] P. Sudarsanam, B. Hillary, M.H. Amin, S.B.A. Hamid, S.K. Bhargava, Appl. Catal. B–Environ. 185 (2016) 213–224.
[10] B. Govinda Rao, P. Sudarsanam, A. Rangaswamy, B.M. Reddy, Catal. Lett. 145 (2015) 1436–1445.
[11] L. Geng, J. Song, Y. Zhou, Y. Xie, J. Huang, W. Zhang, L. Peng, G. Liu, Chem. Commun. 52 (2016) 13495–13498.
[12] U. Schubert, Chem. Soc. Rev. 40 (2011) 575–582.
[13] L. Qi, Q. Yu, Y. Dai, C. Tang, L. Liu, H. Zhang, F. Gao, L. Dong, Y. Chen, Appl. Catal. B: Environ. 119–120 (2012) 308–320.
[14] J. Yang, L. Lukashuk, H. Li, K. Foettinger, G. Rupprechter, U. Schubert, Catal. Lett. 144 (2014) 403–412.
[15] J. Yang, J. Ofner, B. Lendl, U. Schubert, Beilstein J. Nanotechnol. 7 (2016) 1815–1821.
[16] Z. Xiao, C. Wu, L. Li, G. Li, G. Liu, L. Wang, Int. J. Hydrogen Energy 42 (2017) 5606–5618.
[17] T. Osaki, J. Sol-Gel Sci. Technol. 82 (2017) 133–147.
[18] A.K. Chaudhari, V.B. Singh, Arabian J. Chem. (2016), http://dx.doi.org/10.1016/j.arabjc.2016.11.007 (Ahead of Print).
[19] J.E. Powell, J.L. Farrell, Rare Earth Res. Seminar, Lake Arrowhead Calif. 1960, 1961, pp. 26–30.
[20] B. Ksapabutr, E. Gulari, S. Wongkasemjit, Mater. Chem. Phys. 83 (2004) 34–42.
[21] D. Andreescu, E. Matijevic, D.V. Goia, Colloids Surf. A 291 (2006) 93–100.
[22] B. Ksapabutr, E. Gulari, S. Wongkasemjit, Mater. Chem. Phys. 99 (2006) 318–324.
[23] M. Rumruangwong, S. Wongkasemjit, Appl. Organomet. Chem. 22 (2008) 167–170.
[24] S. Biswas, K. Mullick, S.-Y. Chen, A. Gudz, D.M. Carr, C. Mendoza, A.M. Angeles-Boza, S.L. Suib, Appl. Catal. B: Environ. 203 (2017) 607–614.
[25] B. Chen, L. Wang, S. Gao, ACS Catal. 5 (2015) 5851–5876.
[26] B. Chen, J. Li, W. Dai, L. Wang, S. Gao, Green Chem. 16 (2014) 3328–3334.
[27] S. Sithambaram, R. Kumar, Y.-C. Son, S.L. Suib, J. Catal. 253 (2008) 269–277.
[28] E. Beche, P. Charvin, D. Perarnau, S. Abanades, G. Flamant, Surf. Interface Anal. 40 (2008) 264–267.
[29] B. Chen, Y. Ma, L. Ding, L. Xu, Z. Wu, Q. Yuan, W. Huang, J. Phys. Chem. C 117 (2013) 5800–5810.
[30] C. Zhao, Y. Xu, Top. Catal. 60 (2017) 446–458.
[31] H.A. Hansen, C. Wolverton, J. Phys. Chem. C 118 (2014) 27402–27414.
[32] X.-P. Wu, X.-Q. Gong, G. Lu, Phys. Chem. Chem. Phys. 17 (2015) 3544–3549.
[33] D. Fernandez-Torre, K. Kosmider, J. Carrasco, M.V. Ganduglia-Pirovano, R. Perez, J. Phys. Chem. C 116 (2012) 13584–13593.
[34] M. Molinari, S.C. Parker, D.C. Sayle, M.S. Islam, J. Phys. Chem. C 116 (2012) 7073–7082.
[35] K.S.W. Sing, D.H. Everett, R.A.W. Haul, L. Moscou, R.A. Pierotti, J. Rouquerol, T. Siemieniewska, Pure Appl. Chem. 57 (1985) 603–619.
[36] J.M. López, A.L. Gilbank, T. García, B. Solsona, S. Agouram, L. Torrente-Murciano, Appl. Catal. B: Environ. 174 (2015) 403–412.